IIM METAL NEWS

(MONTHLY EDITION)

CELEBRATING PLATINUM JUBILEE OF IIM

ISSN 0972-0480 *Vol. 25 No. 2* *FEBRUARY 2022*

IIM
Metallurgy
Materials Engineering

THE INDIAN INSTITUTE OF METALS

The Indian Institute of Metals


STEEL FACTS
Steel scrap from lower value steel products can be
converted into high value steels
by using appropriate processing and metallurgy.
For other materials this is not typically possible; in the case of concrete, wood and aluminium the quality of recycled material is often downgraded or downcycled and the material has a limited number of lives.
worldsteel.org

IIM METAL NEWS

Vol. 25 No. 2 February 2022

CONTENTS

Printed and Published by Shri Kushal Saha, Secretary General, on behalf of "The Indian Institute of Metals", and printed at Print Max, 44, Biplabi Pulindas Street, Kolkata-700009 • Email : printmax41@gmail.com and published at 'Metal House', Plot 13/4, Block AQ, Sector V, Salt Lake, Kolkata-700091, West Bengal, India
E-mail: secretarygeneral.iim@gmail.com, iimmetalnews@yahoo.com Phone: 033-2367 9768 / 2367 5004
Website: www.iim-india.net Fax: (033) 2367 5335
Facebook - https://www.facebook.com/TheIndianInstituteofMetals/
Instagram - https://www.instagram.com/indianinstituteofmetals/
LinkedIn - https://www.linkedin.com/company/the-indian-institute-of-metals/
Twitter - https://twitter.com/iimetals_india

Chief Editor : Dr N Eswara Prasad

THE INDIAN INSTITUTE OF METALS

PATRONS

Mr R M Dastur Dr Baba Kalyani

ADVISORY COMMITTEE OF FORMER PRESIDENTS

Dr Dipankar Banerjee
Mr M Narayana Rao
Mr H M Nerurkar
Prof K Chattopadhyay
Dr R N Patra
Mr S S Mohanty
Mr T V Narendran, Convenor
Prof Indranil Manna
Dr Biswajit Basu
Mr Anand Sen

COUNCIL FOR THE YEAR 2021-22

PRESIDENT
Mr T V Narendran

VICE PRESIDENT & CHAIRMAN
Metal Science Division
Dr Samir V Kamat

VICE PRESIDENT & CHAIRMAN
Non- Ferrous Division
Mr Satish Pai

VICE PRESIDENT & CHAIRMAN
Ferrous Division
Mr Sajjan Jindal

IMMEDIATE FORMER PRESIDENT
Prof Amol A Gokhale

SECRETARY GENERAL
Mr Kushal Saha

HON TREASURER
Mr Somnath Guha

CONTROLLER OF EXAMINATIONS
Prof P K Mitra

CHIEF EDITOR, TRANSACTIONS
Prof B S Murty

CHIEF EDITOR, IIM METAL NEWS
Dr N Eswara Prasad

Jt. SECRETARY
(Office of President)
Mr Chaitanya Bhanu

MEMBERS

Prof Amit Arora
Dr R Balamuralikrishnan
Prof Suddhasatwa Basu
Dr A N Bhagat
Dr Raghavendra R Bhat
Dr Amit Bhattacharjee
Dr Debashish Bhattacharjee
Dr Tanmay Bhattacharyya
Dr S P Butee
Dr Indranil Chattoraj
Mr B K Das
Mr Prem Ganesh
Mr Kanak Kumar Ghosh
Prof Dipti Gupta
Dr S K Jha
Dr J Krishnamoorthi
Mr Kishore Kumar Mehrotra
Mr Arun Mishra
Prof B K Mishra
Mr Bibhu Prasad Mishra
Dr Suman Kumari Mishra
Prof Sushil K Mishra
Prof Rahul Mitra
Ms Soma Mondal
Dr S V S Narayana Murty
Mr M K Murugan
Mr K Nagarajan
Dr Vinod Nowal
Mr Dilip Oommen
Mr Ambika Prasad Panda
Mr Sudhanshu Pathak
Dr Divakar Ramachandran
Dr Asim K Ray
Dr G Madhusudhan Reddy
Mr Barun Roy
Mr Bhaskar Roy
Prof Rajiv Shekhar
Dr Bimal P Singh
Dr Arijit Saha Podder
Dr S Savithri
Shri Sanjay Sharma
Mr Arun Kumar Shukla
Prof Amarendra Kumar Singh
Mr Brijendra Pratap Singh
Mr Lokendra Raj Singh
Dr T Sundararajan
Mr G Surendra
Prof Satyam Suwas
Dr Vilas Tathavadkar
Dr M Vasudevan
Dr P V Venkitakrishnan

FORMER PRESIDENTS

1946-48	Late J J Ghandy	1977-78	Late V A Altekar	1992-93	Late A C Wadhawan	2007-08	Late Srikumar Banerjee
1948-50	Late P Ginwala	1978-79	Late T R Anantharaman	1993-94	Late R Krishnan	2008-09	Mr L Pugazhenthy
1950-52	Late Phiroz Kutar	1979-80	Late P L Agrawal	1994-95	Dr S K Gupta	2009-10	Dr Sanak Mishra
1952-54	Late G C Mitter	1980-81	Late EG Ramachandran	1995-96	Mr R N Parbat	2010-11	Dr D Banerjee
1954-56	Late M S Thacker	1981-82	Late C V Sundaram	1996-97	Late P Rodriguez	2011-12	Mr M Narayana Rao
1956-58	Late K S Krishnan	1982-83	Late Samarpungavan	1997-98	Late S Das Gupta	2012-13	Mr H M Nerurkar
1958-60	Late S K Nanavati	1983-84	Late J Marwaha	1998-99	Dr C G K Nair	2013-14	Prof K Chattopadhyay
1960-62	Late G K Ogale	1984-85	Late A K Seal	1999-00	Prof S Ranganathan	2014-15	Dr R N Patra
1962-65	Late Dara P Antia	1985-86	Dr J J Irani	2000-01	Mr V Gujral	2015-16	Mr S S Mohanty
1965-67	Late B R Nijhawan	1986-87	Late Y M Mehta	2001-02	Late P Parvathisem	2016-17	Prof Indranil Manna
1967-70	Late M N Dastur	1987-88	Dr V S Arunachalam	2002-03	Late P Ramachandra Rao	2017-18	Dr Biswajit Basu
1970-72	Late Brahm Prakash	1988-89	Late S R Jain	2003-04	Late S K Bhattacharyya	2018-19	Mr Anand Sen
1972-74	Late P Anant	1989-90	Late L R Vaidyanath	2004-05	Dr T K Mukherjee	2019-20	Dr U Kamachi Mudali
1974-76	Late FAA Jasdanwalla	1990-91	Dr P Rama Rao	2005-06	Late Baldev Raj	2020-21	Prof Amol A Gokhale
1976-77	Late S Visvanathan	1991-92	Dr T Mukherjee	2006-07	Mr B Muthuraman		

FORMER SECRETARIES / SECRETARY GENERALS*

1946-57	Late Dara P Antia	1968-76	Dr M N Parthasarathi	1986-97	Late S S Das Gupta	2006-13	*Mr J C Marwah
1958-67	Mr R D Lalkaka	1977-86	Late L R Vaidyanath	1997-06	Mr J C Marwah	2013-15	*Mr Bhaskar Roy
						2015-18	*Mr Sadhan Kumar Roy

Late Dr. Subir Kumar Bhattacharyya (1945 - 2022)
IIM President (2003-04)

With a deeply pained and heavy heart we convey that Dr. Subir Kumar Bhattacharyya, Former President (2003-2004) and Honorary Member of the Indian Institute of Metals had left for the heavenly abode.

Dr. Subir Kumar Bhattacharyya graduated with Metallurgical Engineering in 1966 from the then Bengal Engineering College, Shibpur. He did his Ph.D from Massachusetts Institute of Technology (MIT), USA. Thereafter He joined Alloy Steels Plant, Durgapur in 1974 in the Research and Development wing and later became in-charge of the same department. The development of Hadfield Steel Plates and coloured stainless steels were some of his notable achievements.

In 1988, he joined R & D Centre for Iron & Steel (RDCIS), Ranchi - the R & D wing of SAIL. He went on to become Director, RDCIS. He took charge as the Managing Director of Durgapur Steel Plant in 2001 and he superannuated in December, 2005. He played a major role in the all-round development of DSP, turning the perennially loss-making plant into a profit-making vibrant Organisation. Under his leadership, the rated capacities of major shops were surpassed while there were improvements also in the major techno-economic parameters. He led from the front for the development of special steels in DSP and guided the making of new value-added products thereby creating new marketing opportunities.

He had to his credit 50 publications in national and international journals of repute as well as 5 Indian and foreign Patents. He had been closely associated with various educational institutions. Starting with Gold Medal in 1966 from BE College, Dr. Bhattacharyya won many Awards and Distinctions. In 1984, he received the National Metallurgists' Day Award of IIM. Other notable Awards & Distinctions are Distinguished Alumnus Award of BE College in 1989, OP Jindal Gold Medal Award of IIM in 1997, Life Fellow of IIM in 1996, Member of National Academy of Engineering [INAE] in 1997.

During his long association with IIM starting as a Student Member in 1961, Dr. Bhattacharyya took keen interest in the activities of IIM all along. He served IIM in various capacities: as Member, Chapter Secretary, Chapter Chairman, Council Member, Vice President and Chairman of Ferrous Division before taking up the baton as President in 2003. His stewardship as the Chairman of the Administrative cum Finance Review Committee [AFRC] till 2019 was characterized with diligent efforts, invaluable suggestions to the Institute's management in order to enhance the credibility and visibility of the Institute. By all measures, the administrative framework of the Institute has improved immensely during his tenure as President, and also as Chairman, AFRC.

We remember Dr. Bhattacharyya as an affable person and a simple soul. We join the bereaved family in praying to the Almighty to grant the departed soul to rest in peace, and give his family enough strength and courage to bear this irreparable loss.

Retrogression and Re-Ageing treatment of AA7010 Alloy Forgings

Mrudula Prashanth[1] and R Raghavendra Bhat[2]

Keywords: Aluminium alloy (AA7010), RRA heat treatment, SCC resistance, T77 Temper, Ultimate Tensile Strength, Electrical Conductivity.

Abstract

AA7010 Al-alloy is a unique material in 7XXX series, mainly used in industries such as aircraft and automobile, as they have a high strength-to-weight ratio. If the alloy is utilized for long term, the alloy is prone to corrosion fatigue, exfoliation corrosion, and stress corrosion cracking (SCC). The alloy which is subjected to T6 temper condition exhibits a high strength but is vulnerable to SCC. To avoid this situation, a multi-stage heat treatment process known as Retrogression and Re-aging (RRA) was instituted, in which the alloy is subjected to T6 temper condition followed by a thermal cycle containing two stages. Stage I is known as retrogression, which includes heating to a high temperature for a small period of time followed by quenching. In stage II, the alloy is re-aged at a temperature equivalent to that of T6 condition. This multi-stage process thus provides good ultimate tensile strength and comparatively good SCC resistance. In the present work, AA7010 alloy forgings were subjected to T6 condition and then retrogressed in a salt bath furnace at 200±3 ^{0}C and 210±3 ^{0}C for 30 to 90 minutes with an increment of 10 ^{0}C except 80 minutes. The process was followed by re-aging. The alloy treated by the method at 200±3 ^{0}C for 40 minutes gave optimal result with respect to UTS and resistance to SCC.

1. Introduction

7XXX series alloys have been used in aircraft structural applications due to their high strength, low density and excellent mechanical properties developed by artificial aging process [1].

In critical aerospace applications and automobiles, the need for high strength and excellent mechanical properties led to the development of Al-Zn-Mg-Cu alloy AA7010 (DTD5636) during late 1970's, but the high strength Al-alloys such as 7xxx series in T6 temper condition are of concern, as they are prone to undesirable stress corrosion cracking, especially in major structural components in aircraft. It is seen that the poor resistance to SCC in 7XXX Aluminium alloy series has been overcome by subjecting the alloy to over-aged temper condition (T73), but this reduces the material strength to about 9-16% in comparison to T6 condition. An RRA process which is a multi-stage heat treatment process, was introduced to overcome this deficiency of combined corrosion resistance and strength. The response of RRA thermal treatment for aluminium 7XXX series alloys was found to be extremely good [2].

This article presents the findings on the influence of RRA thermal treatment on the various properties such as mechanical properties and resistance against stress corrosion cracking. This was affirmed by carrying out conductivity tests on forgings. The investigations were conducted on the specimen extracted from forgings in

[1] **Department of Mechanical Engineering, Amrita School of Engineering, Amrita Vishwa Vidyapeetham, Bangalore campus, Bangalore-560037, E-mail: *p_mrudula@blr.amrita.edu*.**

[2] **Additional General Manager (Retired), Foundry and Forge Division, HAL, Bangalore, India, E-mail: *rr_bhat@yahoo.co.uk***

conformance with the standard methods. Prior to retrogression treatment, the samples were subjected to T6 condition. Later, the samples were retrogressed in a furnace containing salt bath at 200±3 ^{0}C and 210±3 ^{0}C for a period varying from 30 to 90 minutes with an increment of 10 ^{0}C except for 80 minutes. The study was intended to arrive at an optimized retrogression temperature and to establish a heat treatment cycle that gave the best combination of SCC resistance and strength.

2. Experimental Procedure

A forged bar (200 mm x 500 mm x 70 mm) was taken as the raw material for study. The samples were prepared by cutting to a size of (20 mm x20 mm x70 mm) along the short transverse (ST) direction. Each trial consisted of a set of 15 samples. The chemical composition of the forged samples was checked and confirmed using a computerized Spectrovac chemical analyzer. The actual composition of the alloy was as tabulated in Table1. The results of the analysis showed that the constituents were in conformed with the standard specification.

2.1 Heat treatment Cycle

The current work used heat treatment cycles at 3 different tempers T6, T74 and T77 (RRA).

The T6 temper treatment procedure is as follows: the samples were solutionized in a pit furnace at 480±5 ^{0}C and immediately water-quenched without any delay, followed by artificial aging at 120±3 ^{0}C for 24 h.

The pilot process was to bring all the specimens to T6 temper condition. Later the samples were subjected to retrogression at 200±3^{0}C and 210±3 ^{0}C for a duration of 30, 40, 50, 60 and 90 minutes and immediately quenched in water without any delay. Further, these samples were subjected to re-aging in an electric resistance furnace at 120±3 ^{0}C for a period of 24 h and cooled in air: the same aging condition as that of T6 temper. This is termed as T77 temper and is popularly known as RRA.

T74 temper is obtained by first solutionizing the specimen and then subjecting the specimen to two stages of aging process: the first stage is heating to 110±3^{0}C for 8 h and 175±3^{0}C for 14h [3].

2.2 Testing Equipment

The specimens subjected to three different heat treatment cycles were further tested for various properties: hardness, electrical conductivity, ultimate tensile strength (UTS), yield strength (YS) and % elongation. A Universal hardness testing machine (INDENNTEC make) was used to check the specimen (sample) hardness on Brinell hardness scale using a tungsten carbide indenter and a ball having a diameter of 2.5 mm with an applied load of 62.5 kg providing 10 s of dwell time. Conductivity meter type 978 was used for measuring the electrical conductivity and the meter has a measurement range of (10-120) % IACS, the tensile properties were evaluated as

Table 1: Chemical composition of the 7010Al-alloy forgings

Elements	Values obtained (%)	Specification requirement
Zn	5.84	5.70-6.70
Mg	2.26	2.10-2.60
Cu	1.53	1.50-2.00
Fe	0.13	0.15 max
Si	0.10	0.12 max
Mn	0.04	0.10 max
Ni	0.01	0.05 max
Zr	0.12	0.11-0.17
Other elements	Within limits	0.05 each; Total - 0.15
Al	Remainder	

per ASTM-E8/E8M standard, and the tests were carried out at room temperature using TIRA testing machine.

3. Results and Discussion

3.1 RRA and its effects on properties of the alloy

All the data in this note pertain to T6, T74 as well as T77 conditions and plotted to compare with each other, wherein the T6 and T74 values correspond to one temperature; while in the case of T77 temper, the values are evaluated and compared at and for different temperatures.

The properties of the samples were tested at T6 condition along the short transverse (ST) direction; they were: Hardness: 173 HBW, Electrical conductivity: 31.29% IACS, UTS-527 N/mm2, 0.2% Yield Strength:-448 N/mm^2 and % elongation :- 3.7. Likewise, the properties, tested at T74 condition along ST direction, are as follows: Hardness-152.3 HBW, Electrical Conductivity -40.74% IACS, UTS-471 N/mm^2, 0.2% Yield strength - 394 N/mm^2, % Elongation- 2.4.

3.1.1 Hardness at varying tempers

Figure 1 shows the variation of hardness at different regression times for two retrogression temperatures and compared with two other tempers viz. T74 and T6. With the increase in temperature, it is found that the hardness decreases gradually with increase in the retrogression time. A higher hardness than T74 condition is achieved at all conditions when treated at 200 ± 3 ^{0}C. The behaviour of hardness is similar at 210±3 ^{0}C as well, except at 90 minutes of retrogression time. The hardness of the alloy decreases with an increase in retrogression temperature and time.

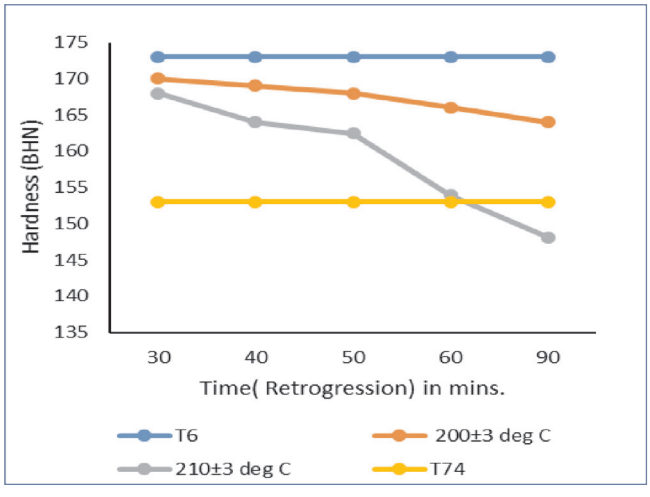

Fig. 1 : Hardness Vs Retrogression time

A detailed study of the graph reveals that at retrogression temperature of 200±3 ^{0}C (RRA200) and 210±3 ^{0}C (RRA210), hardness achieved is maximum at a regression time of 30 minutes and the hardness decreases for the other regression times of 40, 50, 60 and 90 minutes.

3.1.2 Electrical Conductivity at varying tempers

Electrical conductivity is one of the significant and independent parameter to identify the response of material towards heat treatment amongst aluminium alloys in the process of age-hardening. During retrogression and aging/ re-aging, the electrical conductivity varies depending on the distribution of precipitate phases and its size. In 7XXX series of aluminium alloys, SCC is considered as a function of the electrical conductivity. In the current study of AA7010 alloy forgings, if the material is able to achieve electrical conductivity of 38-40% IACS, it is regarded as a material with an improved SCC-resistance.

Figure 2 shows the relationship of electrical conductivity with retrogression time at varying temper conditions. At both 200 RRA and at 210 RRA, electrical conductivity is found to be increasing with increase in retrogression time.

It is observed that for 40 minutes of retrogression time, the electrical conductivity is approximately equal to T74 condition at both retrogression temperatures of RRA200 and RRA210. A higher electrical conductivity is achieved in RRA210 than compared to T74 condition for retrogression time crossing 40 minutes.

RRA200 showed similar electrical conductivity with that of T74 temper but it is slightly lower than that of 210±3^{0}C at all retrogression times. But the behaviour is in total contrast with that of hardness and they are inversely proportional to each other i.e. with an increase in electrical conductivity, hardness decreases.

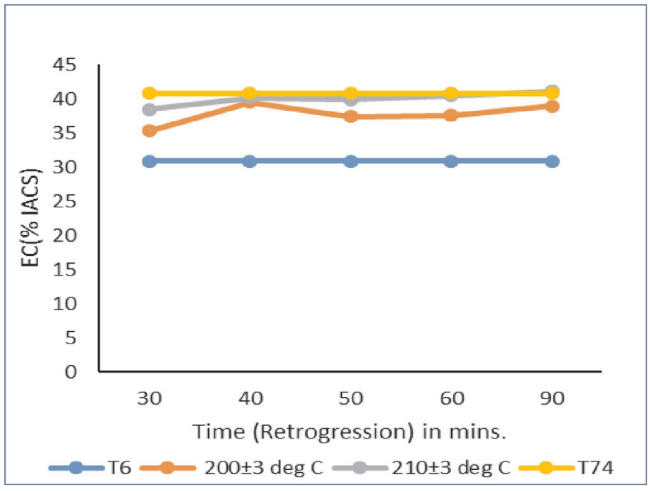

Fig. 2 : Electrical conductivity (EC) Vs Retrogression time.

3.1.3 Ultimate Tensile Strength (UTS) at varying tempers

The UTS of the alloy AA7010 is found to decrease with increasing retrogression temperature and times excluding 50 minutes of retrogression time where it marginally increases. Figure 3 shows the way UTS of AA7010 Al alloy forgings has been influenced by RRA. At both RRA200 and RRA210, the UTS is found to be higher than T74 temper up to 60 minutes of retrogression time.

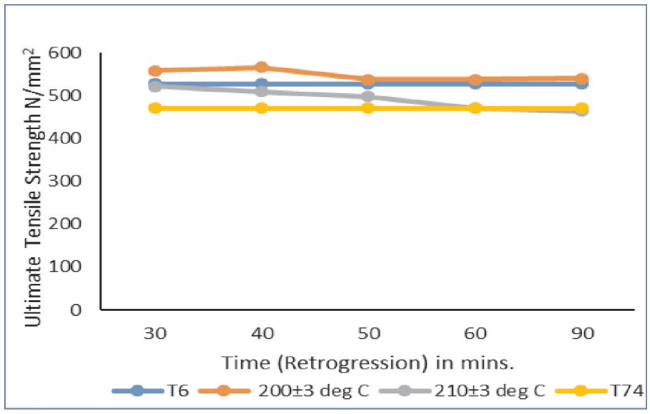

Fig. 3 : UTS Vs Retrogression time

3.1.4 Yield Strength (YS) at varying tempers

Figure 4 below explains how yield strength is influenced by variation in RRA. It is calculated as 0.2% offset strain. The curve explains the reduction in the yield strength with the increment in retrogression temperature and time as referred to 210±3 ^{0}C retrogression temperature curve. A significant outcome is that the yield strength at all retrogression times is higher than T74 temper when retrogressed at 200 ±3 ^{0}C. Yield strength is found to be equal or marginally higher than T6 condition for a retrogression temperature of 200±3 ^{0}C, when retrogression time lies between 30-50 minutes and the relationship between Yield strength and the retrogression time is as depicted in fig 4.

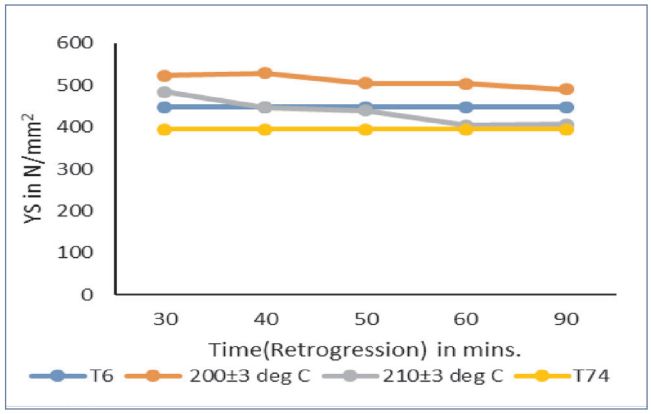

Fig. 4 : Yield Strength (YS) Vs Retrogression time at varying tempers.

3.1.5 % Elongation at varying tempers

% Elongation Vs. retrogression time at varying temper conditions is plotted in Fig.5. The % elongation is found to be higher than with T74 at both RRA temperatures. Further, when compared with T6 temper condition, the % elongation is found to be higher above 40 minutes of retrogression time at RRA200 and RRA210. This indicates an ample improvement in ductility of the RRA-treated specimen.

3.2 Discussion

The forgings of AA7010 Al alloy which were retrogressed at 200 ±3 ^{0}C exhibited more consistent results and helpful properties when tested for electrical conductivity, hardness, and mechanical properties.

The findings are outlined as follows. The hardness of the 164 HBW is achieved which is higher than (153 HBW) T74 condition. The electrical conductivity achieved was 39.50% IACS which is close to 40.8% IACS observed for T74 condition and was much higher than T6 (30.9% IACS) condition. The UTS of 501 N/mm2, YS of 446 N/mm2 and elongation of 4.40% are achieved, which

is greater than T74 temper condition and close to T6 temper. Therefore, retrogression carried out at 200±3 ^{0}C for 40 minutes, heat treated with RRA condition was found to be the best choice of temperature and time for the heat treatment which provides the best results considering the parameters such as UTS, hardness and conductivity.

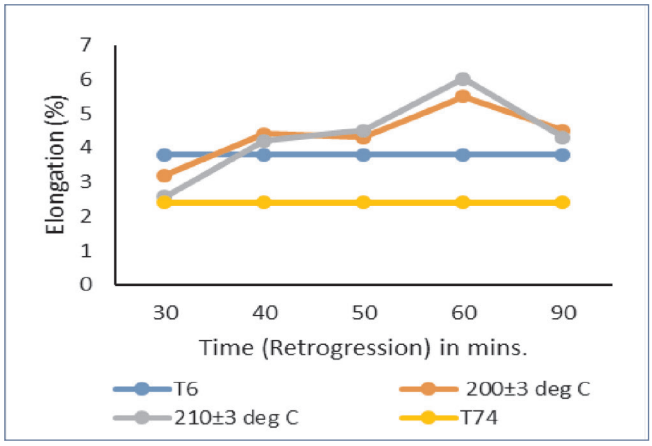

Fig. 5 : Elongation(Percentage) Vs retrogression time at different tempers.

From literature, it is evident that due to RRA, copper enrichment and coarsening of grain boundary precipitates occur, which reduces the rate of corrosion reaction. Due to this, a potential difference (PD) is created between the grain boundary and the grain interior which plays a major role in improving SCC resistance [4] or any other corrosion process. This variation in potential difference leads to a change in the electrical conductivity. Hence, the electrical conductivity directly can be related to stress corrosion cracking (SCC) and to quantify the resistance to SCC.

The microstructure of 7XXX series Aluminium alloys consists of the following precipitate morphology: MgZn2 S- Equilibrium precipitate, S/- the metastable precipitate and GP (Guinier-Preston) zones [5-8]. The microstructure of the samples treated at T6 temper condition consists of metastable phase S/ [6-9] in a very small proportion but greatly filled with GP zones.

From the previous research work in the field [9-12], it is found that that the dissolution of GP zones occurs partially and a fine metastable precipitate formation S/ occurs in the grains of Al-matrix which are re-precipitates upon re-aging, wherein the S precipitate forms and their growth is seen at the grain boundary. Hence the hardness is found to reduce when subjected to retrogression. Further, a very fine distribution of S/phase is seen in the grains of Al-matrix which is comparable with T6 treated condition. Hence it is concluded that the existence of S/ particles and its volume fraction are responsible for the peak strength achieved. In continuation, clustering and coalescence of precipitates are seen which are responsible for reduction in tensile strength and hardness at higher retrogression time and temperature. Also, it is understood that the depletion in the solute occurs which tends to purify the Al-matrix; this purification leads to formation of new precipitates or the pre-surviving precipitates coarsen. This leads to an increase in electrical conductivity upon increase in retrogression time [13].

4. Conclusion

On the basis of alloy response to electrical conductivity, hardness and mechanical properties, it is concluded that the samples retrogressed at 200±3 ^{0}C for 40 minutes employed in the present investigation resulted in the best combination of properties. Similarly, the samples retrogressed at 210±3 ^{0}C showed comparable properties at a retrogression time of 30 minutes. Both these are found to be the optimized RRA parameters for the respective regression temperatures wherein the consistent mechanical properties are achieved without any sacrifice in conductivity, but achieving better SCC resistance.

5. References

[1] Robinson J.S., Cudd R.L., Tanner D.A., Dolan G.P., Quench sensitivity and tensile property in homogeneity in 7010 forgings, Journal of Material Processing Technology, 119, 2001, pp 261-267.

[2] Cina, B and Gan, Reducing the susceptibility of Alloys particularly aluminium Alloys to Stress Corrosion Cracking, Israel Aircraft Industries Ltd., U.S. Patent 3856584, Dec 24,1974.

[3] Aerospace Material Specification, DTD5636, aluminium alloy, Wear, Elsevier Publication, Materials Department, RAE. Farnborough 2004, pp 852-861. Procurement Executive, Ministry of Defence, UK July 1989.

[4] Sarkar B., Mark M., Strake Jr E.A., The effect of copper content and heat treatment on the stress corrosion characteristics of Al-6Zn2Mg-XCu alloy, Metals Trans. A, 1981, 3, 12A, pp1929-1943.

[5] Loffler H., and Kovacs I., and Lendvai V., Review: Decomposition process in Al-Zn-Mg alloys, Journal of Material Science, Volume 18, 1983, pp 2215-2240.

[6] Nguyen Cong Danh, Krishna Rajan, and W., Wallace, A TEM study of microstructural changes during RRA in 7075 aluminium alloy, Metallurgical Transactions A, 1983, 14(A), pp 1843-1850.

[7] Park J.K., Ardell A.J., Effect of Retrogression and Re-aging treatments on the microstructure of Al-7075-T651, Metallurgical Transactions A, 15A, 1984, pp1531-1543.

[8] Berg L. K., Gjonnes, J., Hansen V., Li Z., Knutson-wedel, Waterloo G., Schryvers D., and Wallenberg L.R., GP Zones in Al-Zn-Mg alloys and their role in artificial aging, Acta Materialia, Volume 49, 2001, pp3443-3451.

[9] Antonio Bladantoni, On the microstructural changes during the retrogression and re-aging of 7075 type aluminium alloys, Material Science and Engineering, 72, 1985, pp L5-L8.

[10] Feng Chun, Lui Zhi-Yi ,Ning Ai-lin, LuiYan-bin, Zeng Su-min, Retrogression and re-ageing of Al-99.99%Zn-1.72%Cu-2.5%Mg-0.13% Zr aluminium alloy, Transactions of Non-ferrous Metals Society of China, Volume 16, 2006, pp1163-1170.

[11] Viana, F, Pinto A.M.P., Santos H.M.C., Lopes A.B., Retrogression and re-ageing of 7075 aluminium alloy: microstructural characterization, Journal of Materials Processing Technology, 92-93, 1999, pp 54-59.

[12] Oliveira Jr.A.F., de Barros M.C., Cardoo K.R., Teavessa D.N., The Effect of RRA on the strength and SCC resistance of AA 7050 and AA 7150 aluminium alloys, Material Science and Engineering, A379, 2004, p321-326.

[13] Murat Baydogan, Husey in Cimenoglu, Sabri Kayali, E., A study on sliding wear of a 7075 aluminium alloy, Wear, Elsevier Publication, 2004, pp 852-861.

****

Laser Surface Alloying of Compositionally Graded Coating on Aluminium and Magnesium*

Jyotsna Dutta Majumdar[a1], I Manna[a,b2]

Abstract

The paper presents an earlier research experience on development of compositionally graded surface on magnesium and aluminium by laser surface alloying. Laser surface alloying has been carried out with a high power continuous wave CO_2 laser and simultaneous addition of alloying elements (or mixture) using a nozzle in the molten pool. Ar was used as the shrouding gas. Subsequent to laser surface alloying, a detailed investigation on microstructure, composition and phase analysis were conducted and mechanical properties of the surface were evaluated in details.

1. Introduction

Wear is a frequently encountered failure of engineering materials in service conditions. The property being essentially surface dependent, may be improved by a suitable modification of surface microstructure and/or composition by applying a hard wear resistant coating [1]. Ceramic dispersed metal matrix composite materials usually possess a superior mechanical properties than metals/alloys. However, metal-matrix composite has less ductility. Furthermore, incorporation of a composite layer on the surface by conventional means is not feasible. On the other hand, a high power laser beam may be used as a source of heat to melt the near surface region and subsequent feeding of hard ceramic particles can form a hard particle dispersed metal-matrix composite on the surface of metallic substrate [2]. The volume fraction of the ceramic particles may be changed by a suitable control of laser/process parameters [3,4]. Higher the volume fraction of dispersed particles, superior is the wear resistance of the composite layer [3,4]. Similarly, wear resistance property may be improved by forming an intermetallic dispersed layer on the surface of metallic substrate.

In the present study, laser surface alloying of Mg based alloy (MEZ), Al, Stainless steel and Mild steel has been made with an objective to improve wear resistance property. A detailed study of the microstructure, composition and phases present in the modified zone has been undertaken to observe the effect of laser parameters on the characteristics of the modified zone. The mechanical properties of the modified layer in terms of microhardness and wear resistance have been evaluated in details [6-16].

2. Experimental

2.1 Laser Surface Alloying of Mg Alloy

In the present investigation, MEZ (RE 2%, Zn 0.5%, Mn 0.1%, Zr 0.1%), a commercially available Mg alloy was chosen as substrate material, because of their potential scope for application as automotive components in the engine and gear section.

Laser surface alloying was carried out with a 10 kW continuous wave (CW) CO_2 laser (Model: Rofin Sinar, RS 10000) having a beam diameter of 4 mm (focal point 30 mm above the surface) and Ar as shrouding gas to avoid oxidation during lasing. A relative speed between the laser beam and the specimen was maintained to control the substrate-laser beam interaction time and greater

[a]**Metallurgical and Materials Engineering Department, IIT Kharagpur, Kharagpur, India**
[b]**Birla Institute of Technology, Mesra, Jharkhand 835215.**
E-mail : ***[1]jyotsna@metal.iitkgp.ac.in, [2]imanna@metal.iitkgp.ac.in***
*** "Reprinted specially commemorating the Platinum Jubilee Celebrations of IIM"**

area coverage. To achieve microstructural and compositional homogeneity of the laser treated surface, a 25% overlap between the successive melt tracks was followed. Two successive tracks were applied with a gradually increase in powder feed rate from 10 to 30 mg/s to produce a graded composition. Al and Mn in the weight ratio of 1:1 were used as alloying powders and Nickel powders were used as alloying powders. Shrouding Ar gas flow rate was maintained constant to 6l/min. The alloyed zone was characterized in terms of microstructure (by optical and scanning electron microscope), composition (by energy dispersive spectroscopy) and phase analysis (by X-ray diffractometer). The mechanical property of the alloyed zone in terms of microhardness was determined by a Vickers microhardness tester using a 25g applied load. The pitting corrosion behavior of the laser surface alloyed specimen was also compared with that of the untreated one by calculating the corrosion rate derived from the potentiodynamic anodic polarization study in a 3.56 wt.% NaCl (pH = 5) solution, using standard calomel electrode as reference electrode and platinum as counter electrode [5].

2.2 Laser Composite Surfacing of Al

(a) With SiC particles

Laser composite surfacing of commercially pure Al was carried out with a 10 kW continuous wave (CW) CO_2 laser with a beam diameter of 3.5 mm by melting of commercially pure Al substrate (of dimension: 2cm × 2 cm × 5 mm) with pre-placed SiC layer (particle size 25-50 μm and of thickness 500 μm) on the surface with Ar as shrouding gas to avoid oxidation. Following laser composite surfacing, the microstructure of the composite surfaced layer (both the top surface and the cross section) was characterized by optical and scanning electron microscopy. A detailed analysis of the phase and composition of the composite layer were carried out by X-ray diffractometer and energy dispersive spectroscopy, respectively to conclude on the particle-matrix interfacial reaction. The microhardness of the composite layer (both on the top surface and along the cross sectional plane) was measured by a Vickers microhardness tester using a 25g applied load. Finally, the kinetics of wear of the composite surfaced Al was compared with the as-received one by a Friction and Wear monitor unit (model no.: TR-208-M1) with the specimen as disc and diamond indenter as pin with a 1 kg applied load and 300 rpm wheel speed.

(b) In-situ formation of TiB_2 with K_2TiF_6 and KBF_6

In the present investigation, Aluminum of dimension: 20 mm × 20 mm × 5 mm was chosen as substrate material. The samples were sand blasted prior to laser processing in order to remove oxide scale from the surface. Laser composite surfacing was carried out by melting the surface of sand blasted substrate using a 10 kW continuous wave CO_2 laser (with a beam diameter of 3.5 mm) and simultaneous deposition of a mixture of K_2TiF_6 and KBF_6 (in the weight ratio of 2:1) using Ar as shrouding environment. Powder feed rate was maintained constant to 4g/min. The process variables used for the present study were laser power and scan speed. The specimens were mounted on a CNC controlled X-Y stage which was moved at a speed of 100-500 mm/min. A relative speed between the laser beam and the specimen was maintained to control the substrate-laser beam interaction time and greater area coverage. To achieve microstructural and compositional homogeneity of the laser treated surface, a 25 % overlap between the successive melt tracks was followed. Sufficient time was allowed for each track to reach room temperature before the subsequent lasing operation was resumed to treat the adjacent track. A large number of trials were undertaken using a wide range of laser power and scan speed combination to see the effect of laser parameters on the quality of composite layer. It was found that under a few selected sets of laser parameters a homogeneous and defect-free composite layer was formed. Following laser composite surfacing, the microstructure of the composite layer (both the top surface and the cross section) was characterized by optical and scanning electron microscopy. A detailed analysis of the phase and composition were carried out by X-ray diffractometer and energy dispersive spectroscopy, respectively. The microhardness of

the composite layer (both on the top surface and along the cross sectional plane) was measured by a Vickers microhardness tester using a 100 g applied load. Finally, the kinetics of wear of the composite surfaced Aluminum was compared with that of the as-received one by a Friction and Wear monitor unit (model no.: TR-208-M1) with the specimen as disc and diamond pyramid indenter (120^0) as pin. During wear testing, the pin was allowed to slide over the disk with a 300 rpm wheel speed at an applied load at 1 kg. During wear testing, cumulative depth of wear was measured as a function of time using Winducom 2003 software. Effect of load on the rate of wear was studied. The pitting corrosion behavior of the laser composite surfaced specimen was also compared with that of the untreated one by calculating the corrosion rate derived from the potentiodynamic anodic polarization study in a 3.56 wt.% NaCl (pH = 5) solution, using standard calomel electrode as reference electrode and platinum as counter electrode. Polarization was carried out from –1900 to –900 mV at a scan rate of 2 mV/s. Tafels plot was constituted from the logarithm of the current value as a function of voltage. The slope of the Tafels plot in the linear region in anodic direction is referred to as anodic Tafel constant and the same in cathodic direction is called cathodic Tafels constant. Corrosion current (i_{corr}) was determined from the intersection of these two linear plots. For comparison, a set of sample was laser surface melted to study the effect of only laser surface melting on characteristics and properties of the surface layer.

3. Results and Discussion

3.1 Laser Surface Alloying of Mg Alloy

Microstructure and composition play a crucial role in determining the final property of any component. The unique features of laser surface alloying over conventional processes lies on the fact of rapid quenching effect arising out of the process which produces a refined microstructure confined to a shallow depth from the surface. Figure 1 shows the scanning electron micrograph of the as-received MEZ used in the present study. The microstructure of as-received MEZ consists of coarse grains of Mg with solid solution of Zn, Mn and rare earth element with a complex compound of Mg, Zn and Ce-rich precipitates along the grain boundaries (confirmed by energy dispersive spectroscopy analysis). Figures 2 (a-c) show the scanning electron micrograph of the cross section (with depth) of laser surface alloyed MEZ with Al+Mn lased with a power of 2.5 kW, scan speed of 200 mm/min and powder feed rate of 10-30 mg/s. From Figure 2 it is relevant that the microstructure of the alloyed zone mainly consists of uniform dispersion of precipitates of intermetallics (of Mg + Al and Al+Mn, Ni powders respectively) in the grain refined matrix of MEZ (though the degree of grain refinement is not clear from the micrograph) and it varies with depth from the surface. The microstructure of the top surface is enriched in alloying contents (Al and Mn) having a very large volume fraction of intermetallics with rod-like precipitate morphology (Figure 2a). The volume fraction of the precipitates was found to decrease as the depth from the surface increases (Figure 2b at a depth of 200 μm from the surface). In this regard, it is relevant to mention that the morphology and area fraction of the intermetallic phases were found to vary with laser power and scan speed. On the other hand, the near-interface microstructure is mainly dendrites with a very fine distribution of precipitates in the microstructure (Figure 2c at a depth of 500 μm from the surface). In this regard, it is relevant to mention that this kind of homogeneous and defect-free microstructure with graded composition is formed only for a very narrow range of laser/process parameters. It has been found that if applied power is too high, there is evaporation from the surface leading to formation of surface crater. On the other hand, if the scan speed is too high (at a too low interaction time), an inadequate melting or improper intermixing leads to presence of undissolved particles in the MEZ matrix [5]. Figure 3 shows the variation of Al and Mn content in the alloyed zone with depth from the surface for laser surface alloyed (lased with a power of 2.5 kW, scan speed of 200 mm/min and powder feed rate of 10 –30 mg/s) MEZ with Al+Mn. From Figure 3 it is relevant that Al

and Mn content in the alloyed zone is maximum (Al: 60 at.%, Mn: 12 at.%) near to the surface, remains constant up to a depth of 500 μm, and decreases gradually to 0 at the alloyed zone-substrate interface (to a depth of 1200 μm). This kind of microstructure is beneficial in reducing residual stress distribution with maximum property on the top surface due to maximum enrichment of alloying content near to the surface region. However, the average alloying content at the surface and its distribution with depth was found to vary with laser parameters. It has been found that increase in laser power decreases the average concentration of alloying element and its distribution predominantly, because of increased dilution. In a similar way, increase in scan speed decreases the average composition distribution mainly because of lower powder input at a low interaction time (= beam diameter/scan speed).

A detailed phase analysis was conducted for the laser surface alloyed specimens to identify the phases formed due to laser surface alloying. Figures 4(a,b) show the X-ray diffraction profiles of the top surface of (a) as-received MEZ and the same following laser surface alloying (lased with a power of 2.5 kW, scan speed of 200 mm/min and powder feed rate of 10-30 mg/min) with Al+Mn. The XRD profile of as-received MEZ mainly consists of peaks of Mg with a few un-identified peaks of mainly intermetallics of Mg and rare earth elements (Figure 4a). On the other hand, the XRD profile of laser surface alloyed MEZ with Al+Mn consists of intermetallics of Al and Mn ($MnAl_6$), Al and Mg (Al_3Mg_2), respectively along with a few peaks of pure Mg (Figure 4b).

Figure 5 presents the microhardness profiles for laser surface alloyed MEZ specimens with Al+Mn (lased with a power of 2.5 kW, scan speed of 200 mm/min and powder feed rate of 10-30 mg/s.) as a function of depth from the surface measured on the cross sectional plane. It is relevant to mention that the microhardness of the alloyed zone has increased significantly to as high as 300 VHN as compared to 35 VHN of the as-received one. Moreover, the microhardness of the alloyed zone is maximum at the near-surface region up to 500 μm depth and gradually decreases to a value of 35 VHN at the alloyed zone-substrate interface. Increase in microhardness of the alloyed zone and its distribution was attributed to the formation of intermetallic phases as a result of laser surface alloying and its gradual change in composition with depth. A detailed study has shown that with increase in applied power, the microhardness of the alloyed zone decreases, due to increased dilution. Hence, the improved microhardness is attributed to the presence of intermetallics in the alloyed zone. Furthermore, it may be noted that the improved microhardness in the alloyed zone is beneficial to impart better wear properties.

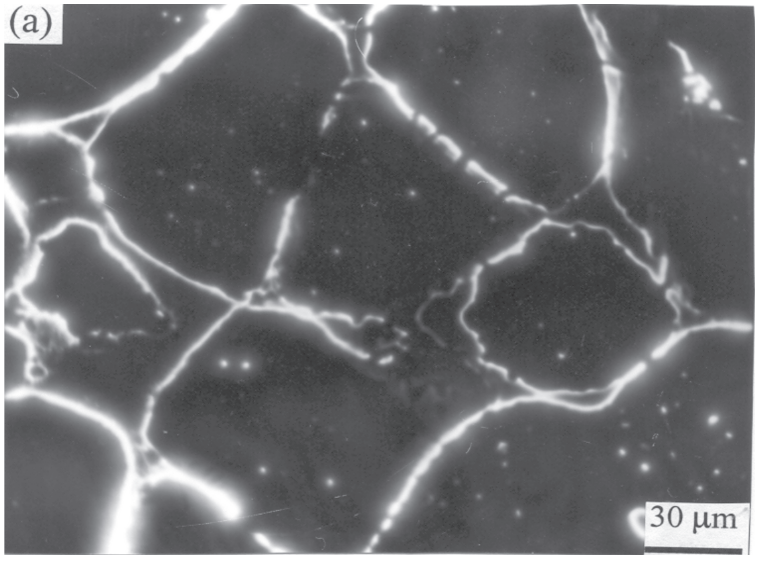

Fig. 1 : Scanning electron micrograph of the as-received MEZ.

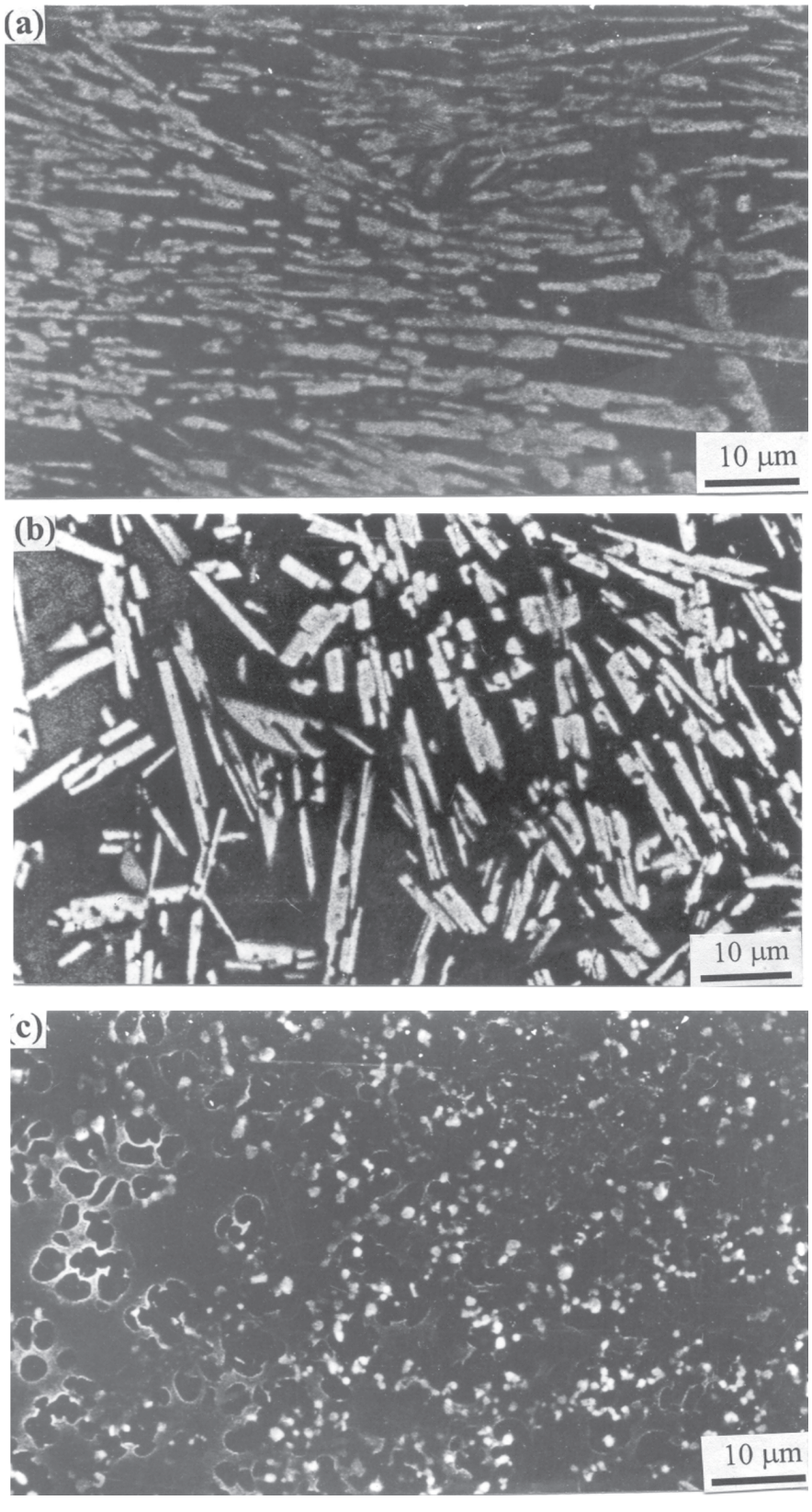

Fig. 2 : Scanning electron micrograph of the cross section of the alloyed zone (a) at the near surface region, (b) intermediate region and (c) near interface region for laser surface alloyed MEZ with Al+Mn lased with a power of 2.5 kW, scan speed of 200 mm/min and powder feed rate of 10-30 mg/s.

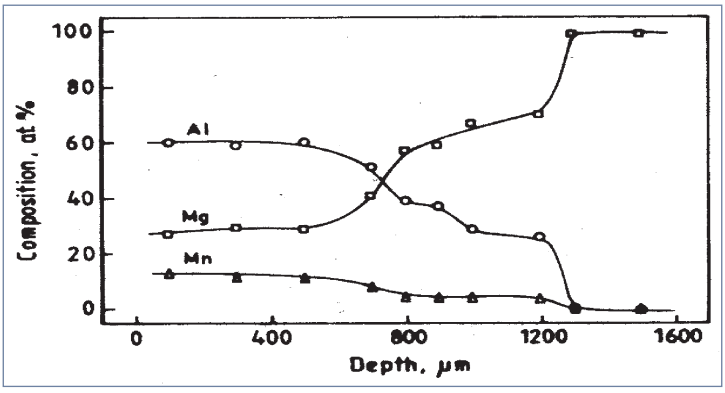

Fig. 3 : Variation of Al and Mn content with depth (along the cross section) in laser surface alloyed MEZ with Al+Mn lased with a power of 2.5 kW, scan speed of 200 mm/min and powder feed rate of 10-30 mg/s.

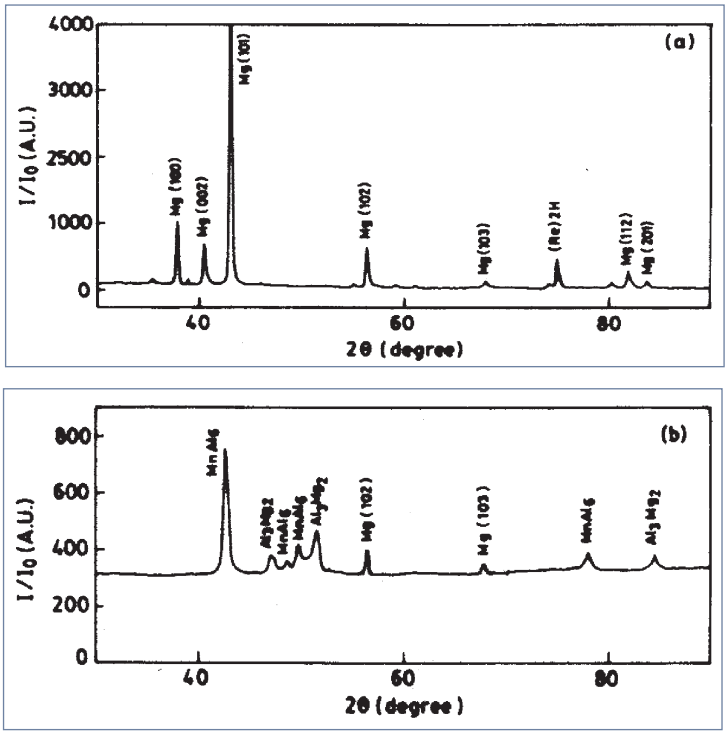

Fig. 4 : X-ray diffraction profile of (a) as-received MEZ and (b) laser surface alloyed MEZ with Al+Mn lased with a power of 2.5 kW, scan speed of 200 mm/min and powder feed rate of 10-30 mg/s.

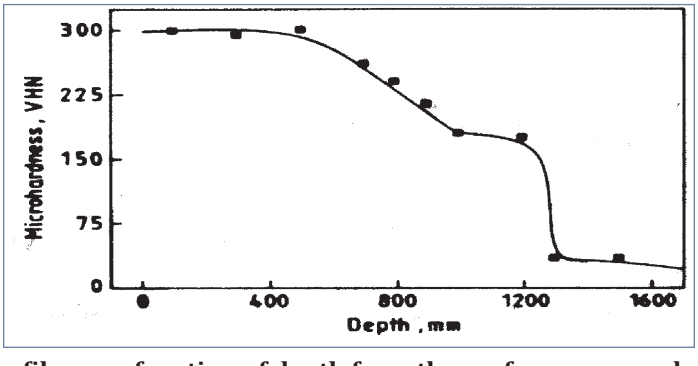

Fig. 5 : Microhardness profiles as a function of depth from the surface measured on the cross sectional plane in laser surface alloyed MEZ with Al+Mn lased with a power of 2.5 kW, scan speed of 200 mm/min and powder feed rate of 20-40 mg/s.

A detailed analysis of the corrosion data in Table 1 reveals that laser surface alloying with Al+Mn has improved the corrosion resistance in a 3.56 wt.% NaCl solution from 25 mm/year (for as-received MEZ) to 7 (in laser surface alloyed MEZ with Al+Mn). A detailed analysis of the microstructure and phase analysis was undertaken to find out the genesis of corrosion and has been discussed elsewhere [13].

Henceforth, it may be concluded that the present laser surface alloying routine is capable of improving the microhardness and resistance to pitting corrosion of MEZ specimen.

3.2 Laser Surface Alloying of Mg with Ni

Fig.6 (a,b) shows the microstructure of (a) As received Mg and (b) the cross section of laser surface alloys Mg (AZ91) with Ni lased with P =2 k W; V=100mm/min.

The Fig 6a consists mainly of coarse grains of Mg and from Fig 6b it is relevant that the width of alloyed is uniform along the cross-section with a sharp and defect free solid-liquid interface.

Fig. 7 shows the microstructure of the top surface of the laser surface alloying of Mg with Ni lased with a power of 2.5 k W, scan speed of 200 mm/min and power feed rate up to of 20 mg/s.

Table 1 : Corrosion behavior of as-received and laser surface alloyed MEZ under different conditions in a 3.56 % NaCl solution

Sample	OCP (mV)	E_{corr} (mV)	I_{corr} (mA)	Corrosion rate (mm per Y)
MEZ (as received)	-1528	-1531	1.714	25
Laser surface alloyed with Al+Mn	-1445	-1448	0.286	7

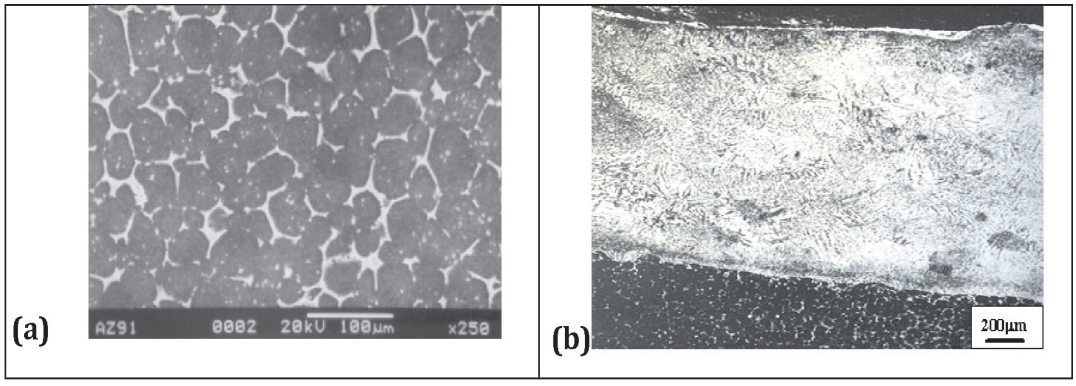

Fig. 6 : The microstructure of (a) As received Mg and (b) the cross section of laser surface alloys Mg (AZ91) with Ni lased with P =2 k W; V=100mm/min

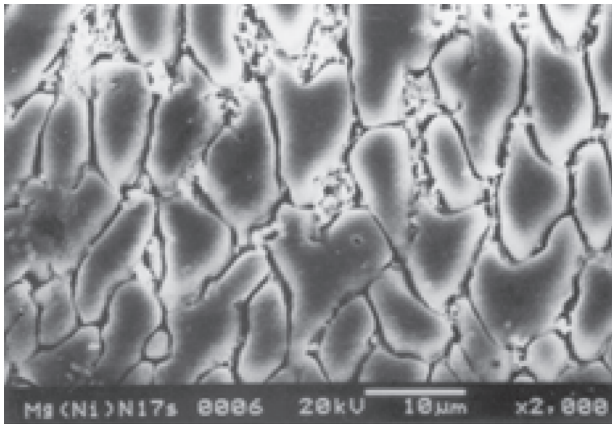

Fig. 7 : The microstructure of the top surface of the laser surface alloying of AZ91 with Ni lased with a power of 2.5 k W, scan speed of 200 mm/min and power feed rate up to of 20 mg/s.

The Fig. 7 mainly consists of precipitation of compound of Mg & Ni in the eutectic mixture of Mg & Ni. The volume fraction of the precipitates was found to vary from 80 to 90 % on the top surface and decreases considerable with depth. The presence of these precipitates makes the matrix very hard. Hence this kind of microstructure is very much useful for wear resistance applications.

Fig. 8 shows the variation of the composition with in laser surface alloy AZ91 with Ni lased with a (a) P =2 k W; V=300mm/min, (b) P= 3 k W; V =100 mm/min, (c) P = 2.5k W; V =400 mm/min respectively.

The concentration of nickel is maximum at the surface and gradually decreases to zero at interface. The gradual change in composition with depth is evident form the microstructure described in the earlier sections. A comparison of Fig 8 (a-c) refers that maximum composition of the alloyed zone at the surface and its distribution with depth is very much dependent on applied process parameters. A detailed study on the variation of average composition of the top surface and its distribution with depth shows the composition of the top surface increase with decreases with decreasing scan speed (because increase power input in the alloyed zone) and decreased power (due to decreased dilution). On the other hand, the composition gradient was found to be steeper with increasing power and increasing scan speed, this attributed the increased temperature gradient with increasing power and increasing scan speed respectively.

A detailed X- ray analysis was conducted on the top surface and as received laser surface alloying of Mg with Ni. To identified the phases formed by laser surface alloying.

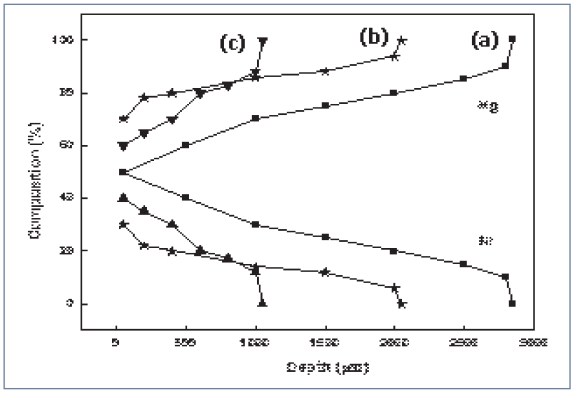

Fig. 8 : The variation of the composition with in laser surface alloy AZ91 with Ni lased with a. (a) P =2 k W; V=300mm/min, (b) P= 3 k W; V =100 mm/min, (c) P = 2.5k W; V =400 mm/min respectively.

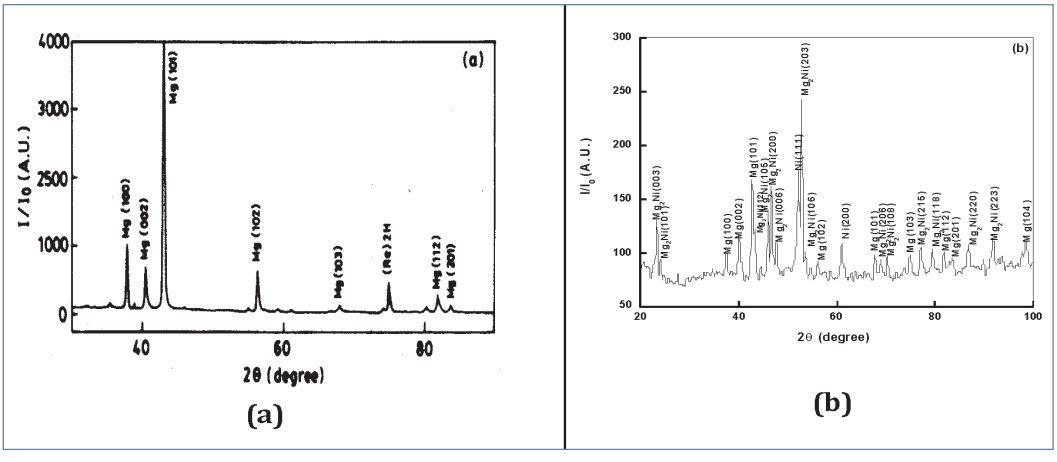

Fig. 9 (a, b) : The X-ray profile of (a) As received Mg and (b) laser surface alloying of Mg with Ni lased at P =2 k W; V=300mm/min.

In Fig9 (a) there is a presence of Mg peaks and in Fig 9(b) there is predominantly of Mg_2Ni.

Fig. 10 shows the Cumulative depth of wear as a function time for (a) As received Mg and (b) Laser Composite surfaced Mg with Ni lased with P=2.5kW and V=300mm/min at 1kg load using diamond indentor.

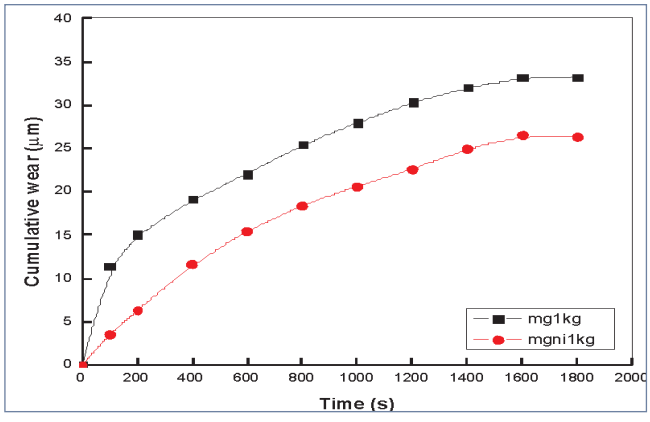

Fig. 10 : The Cumulative depth of wear as a function time for (a) As received Mg and (b) Laser Composite surfaced Mg with Ni lased with P=2kW and V=200mm/min at 1kg load using diamond indentor.

The wear loss of as received and laser surface alloying Mg with Ni corresponding maximizing average hardness value were measured by pin-on-disc wear testing machine against diamond indentor at 1 kg applied load and 15rpm wheel speed for a period of 30 min. From Fig 10 it is noticed that the wear loss is considerably reduced to almost half the value of Mg for laser surface alloying Mg with Ni lased with P =2.5 k W, V= 300 mm /min.

3.3 Laser Composite Surfacing of Al

Figures 11 (a,b) show the optical microstructure of (a) As-received and (b) Laser composite surfaced Al with SiC (lased with a power of 3 kW and scan speed of 500 mm/min) respectively. A comparison between Figure 11(a) and Figure 11(b) shows that laser composite surfacing led to uniform dispersion of the particles in the grain refined Al-matrix. Figure 12 shows the scanning electron micrograph of the top surface of laser composite surfaced Al with SiC (lased with a power of 3 kW and scan speed of 500 mm/min) showing the particle-matrix interface. From Figure12 it is evident that the interface between the particle and the matrix is adherent and defect free. Moreover, the grain boundary regions are full of eutectic product of Al and Si.

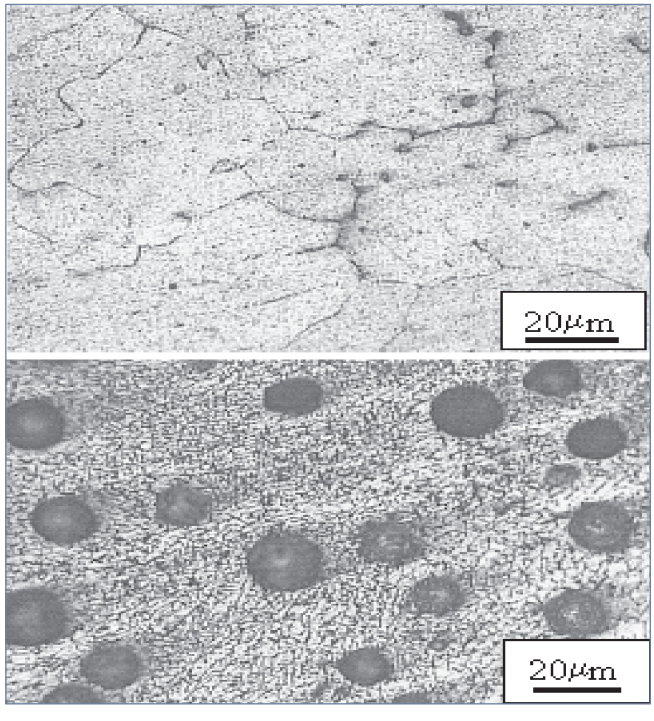

Fig. 11 : Scanning electron micrograph of the top surface of (a) as-received and (b) laser composite surfaced Al with SiC (power= 3 kW and scan speed of 500 mm/min).

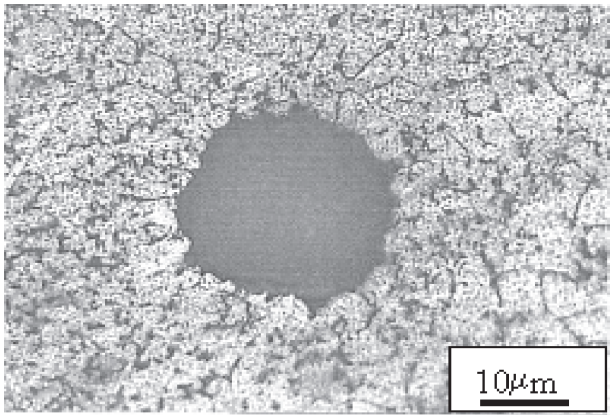

Fig. 12 : Scanning electron micrograph of the particle- matrix interface of the laser composite surface Al with SiC (power = 3 kW and scan speed = 300 mm/min).

Figure 13 (a-b) shows the X-ray diffraction profiles of (a) As-received Al (b) top surface of laser composite surfaced Al with SiC (lased with a power of 3 kW and scan speed of 500 mm/min). A close comparisons of Figure 13(a) and Figure 13(b) show that laser composite surfacing of SiC with Al-matrix lead to dissociation of SiC and subsequent formation of Al_4C_3 and silicon in the matrix. This is also evidence from energy dispersive spectroscopic analysis (Table-1). Hence, SiC particles were totally melted and dissociated leading to the formation of Al_4C_3 particles dispersed into Al-Si matrix. The relative volume fraction of Al_4C_3 and Si was however found to vary with laser parameters. However, a systematic investigation on the variation of individual phases with laser parameters has not been investigated in the present study. Presence of a few Al_2O_3 peaks confirms that though laser composite surfacing was carried out in Argon shroud, oxidation could not be totally avoided.

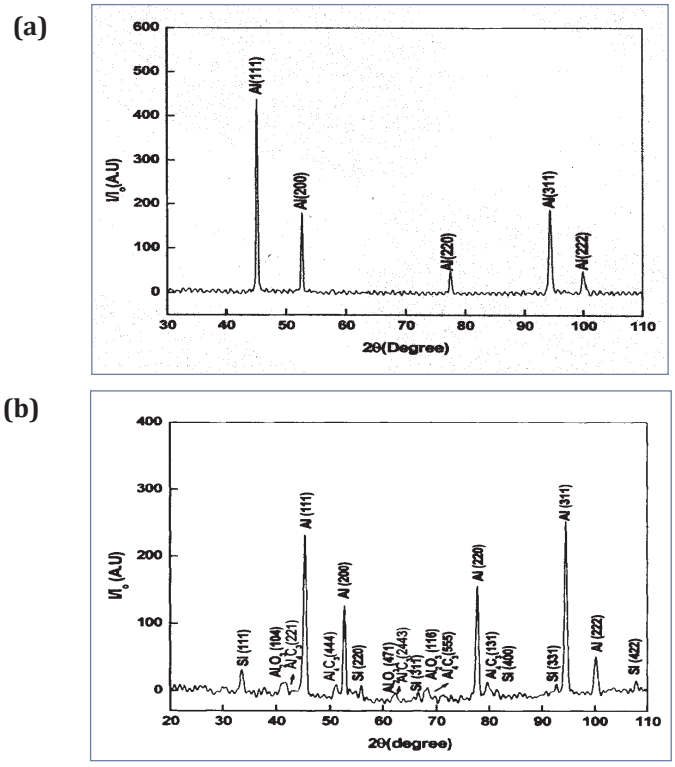

Fig. 13 : X-ray diffraction profile of (a) as-received and the top surface of (b) laser composite surfaced Al with SiC (lased with a power of 3 kW and scan speed of 300 mm/min).

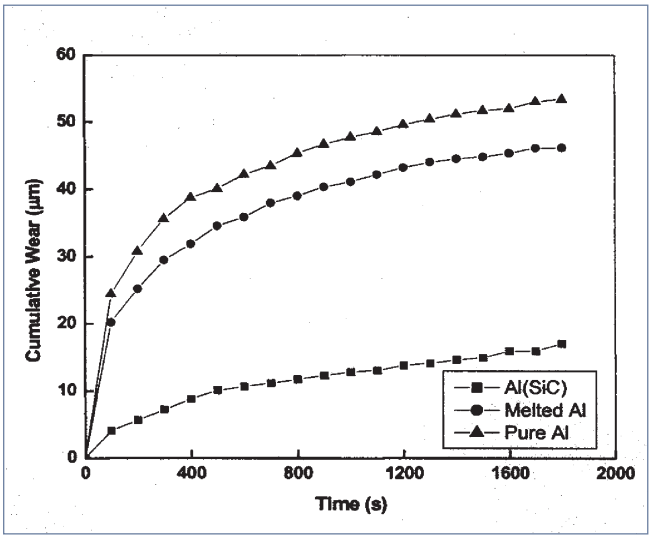

Fig. 14 : Kinetics of wear loss (in terms of depth of wear as a function of time) for as-received, laser surface melted and laser composite surface Al with SiC. (with a power of 3 kW, scan speed of 500 mm/min) against diamond indenter with 1 kg applied load.

Figure 14 shows the wear loss of materials (in terms of depth of wear as a function of time) as a function of time for (1) as-received Al (2) laser surface melted Al (3) laser composite surface Al with SiC (lased with a power of 3 kW, scan speed of 500 mm/min) against diamond indenter with 1 kg applied load. From Figure 14, it is observed that wear loss is maximum in as-received Al followed by same for laser surface melted Al and then laser composite surface Al with SiC. The marginal improvement in wear resistance of laser surface melted Al is because of microhardness improvement attributed to the grain refinement. On the other hand, the superior wear resistance of laser composite surfaced Al with SiC is because of uniform dispersion of hard ceramic particle in refined Al matrix. Hence, it may be concluded that the laser composite surface of SiC on Al has significantly improved the microhardness and wear resistance. Dissociation of SiC caused uniform dispersion of globular Al_4C_3 in Al-Si matrix which is beneficial for improved wear and toughness property as compared to irregular shaped SiC particle dispersion in particle reinforced composite.

4. Summary and Conclusions

From the above-mentioned results and discussion, the following conclusions may be drawn:

Laser Surface Alloying Mg with Zn

1. Laser surface alloying of MEZ with Al and Mn has developed an alloyed zone consists of intermetallics of Al3Mg2 and AlMn6 in the grain refined matrix of MEZ. The morphology is mainly feathery near to the surface, the volume fraction of the precipitates was found to decrease with increasing depth. The microhardness of the alloyed zone has been significantly improved to 300 VHN as compared to 35 VHN of the substrate. Pitting corrosion rate has significantly been reduced to 7 mm/year for laser surface alloyed MEZ with Al+Mn as compared to 25 mm/year of the MEZ substrate.
2. The concentration of Ni is maximum (25 to 50 at.%) at the surface and gradually decreases to zero at the alloyed zone-substrate interface. The maximum composition of the alloyed zone at the surface and its distribution with depth is very much dependent on applied process parameters.
3. The microhardness of the alloyed zone is significantly improved (to 250 to 375 VHN) and is maximum at the surface and decrease gradually with depth (to 35 VHN) at the near interface regions. The maximum microhardness at the surface and its

distributions was found to vary with laser parameters. Microhardness increases with decreasing powers and decreasing scan speed.

4. The corrosion resistance property is increased considerably due to laser surface alloying as compared to as-received AZ91.
5. Laser composite surfacing of Al with SiC has been achieved by melting of preplaced SiC layer on Al surface and subsequently, melting it along with Al. There was formation and dispersion of Al_4C_3 particles in Al matrix. A significant improvement in average microhardness (to 86-100 VHN) and wear resistance (3-4 times) was achieved as compared to that of as-received Al (25 VHN) predominantly due to grain refinement and dispersion of carbides.

Laser Surface Alloying Mg with Mg_2Ni

1. The concentration of alloying material (Ni) is maximum at the surface and gradually decreases to zero at the interface.
2. The maximum composition of the alloyed zone at the surface and its distribution with depth is very much dependent on applied laser process parameters.
3. The microhardness is maximum at the surface and decrease gradually with depth at near interface regions.
4. It is found that the wear resistance is increased by laser surface alloying with Nickel and the wear resistance is increased by 2-3 times than that of the as received Magnesium.

Laser Composite surfaced Al with SiC

1. A significant improvement in average microhardness (185 to 250 VHN) as compared with as received Al
2. The volume fraction of particles are more at top surface and decreased gradually with depth.
3. The wear resistance (3-4 times) was achieved as compared to that of as-received Al

In-situ TiB_2 Formation on Al

1. Significant Improvement in average microhardness (to 75-90 VHN) and wear resistance (2-3 times) was achieved as compared to that of as-received Al (25 VHN) in laser composite surfaced Al with TiB_2.
2. The corrosion resistance property is marginally deteriorated due to the presence of ceramic particles.

References

1. D. R. Gabe, in 'Principles of Metal Surface Treatment and Protection', Pergamon Press, N. York, (1972) 82.
2. Laser Synthesis and Properties of Ceramic Coatings by J. Th. M. Hosson in N. B. Dahotre and T. S. Sudarshan (eds.), Intermetallic and Ceramic Coatings, New York: Marcel Dekker, Inc., 1999. p. 307-440.
3. J. Dutta Majumdar, B. Ramesh Chandra, R. Galun, B. L. Mordike, I. Manna, "Laser Surface Engineering of a Magnesium Alloy with Al + Al_2O_3", *Surf. Coat. Tech.*, 179 (2004) 297-305.
4. J. Dutta Majumdar, B. Ramesh Chandra, R. Galun, B. L. Mordike, I. Manna, "Laser Composite Surfacing of a Magnesium Alloy with Silicon Carbide", Composite Science and Technology, 63 (2003) 771-778.
5. Standard Practice for *Conducting Cyclic Potentiodynamic Polarization Measurements for Localized Corrosion* ASTM Standards, (1961) G61.
6. C.J. Novak In: D. Peckner and I.M. Bernstein, Editors, *Handbook of stainless steels*, McGraw-Hill, New York (1977), p. 1.
7. In: T.W. Clyne and P.J. Withers, Editors, *An introduction to metal matrix composites, Cambridge University Press, Cambridge* (1993).
8. K.G. Budinski, Surface engineering for wear resistance, Prentice-Hall, New Jersey (1988).
9. L.E. Rehn, S.T. Picraux and H. Wiedersich In: L.E. Rehn, S.T. Picraux and H. Wiedersich, Editors, *Surface alloying by ion, electron and laser beams,* ASM, Metals Park, OH (1987), p. 1.

10. B.L. Mordike In: R.W. Cahn, P. Haasan and E.J. Kramer, Editors, *Laser processing of materials, materials science and technology* vol. 15, VCH, Weinheim (1993), pp. 111–136.

11. J. Dutta Majumdar and I. Manna, Laser processing of materials, *Sadhana* **28** (2003), p. 495.

12. J. Dutta Majumdar, B. Ramesh Chandra, R. Galun, B.L. Mordike and I. Manna, Laser composite surfacing of a magnesium alloy with silicon carbide, *Comp Sci Technol* **63** (2003), pp. 771–778.

13. J. Dutta Majumdar, B. Ramesh Chandra, R. Galun, B.L. Mordike and I. Manna, Laser surface engineering of a magnesium alloy with $Al+Al_2O_3$, *Surface Coatings Technol* (2004), pp. 179–297.

14. F.T. Cheng, C.T. Kwok and H.C. Man, Laser surfacing of S31603 stainless steel with engineering ceramics for cavitation erosion resistance, *Surface Coatings Technol* **139** (2001), pp. 14–24.

15. S.C. Tjong and K.C. Lau, Abrasion resistance of stainless-steel composites reinforced with hard TiB2 particles, *Composite Sci Technol* **60** (2000), pp. 1141–1146.

16. C. Dometakis and A. Jha In: R.Y. Lin, Y.J. Chang, R.G. Reddy and C.T. Liu, Editors, *The minerals, metals and materials society* **vol. 420,** Pennsylvania, Commonwealth Drive, Warrendale (1995).

Acknowledgement

Financial help from the Council of Scientific and Industrial Research for the study is gratefully acknowledged.

****

PTC INDUSTRIES LIMITED

Manufacturer of

1) Titanium Castings

2) Nickel Super Alloys Castings

3) Hot Isostatic Pressurised Parts

4) 5 Axis CNC Machining

Components of Aero Engines, Rocket, Missiles, Submarines and Land based Defence equipments.

Advanced Manufacturing and Technology Centre
NH-25A, Sarai Sahjadi, Lucknow – 227101
E-mail – marketing1@ptcil.com ; Ph no. 0522-7111017 ; Fax no. 011-66173715

Corrosion can improve materials' durability

Researchers at Cornell University, Ithaca, N.Y., used advanced atomic modeling to explore the ways environment can influence the growth of cracks in alloys such as aluminum and steel and found when it comes to the integrity of structural alloys, a little corrosion may sometimes be a good thing.

By removing atoms from the tip of a crack, the modeling showed the researchers could prevent a crack from propagating, essentially improving the material's mechanical performance. This could help engineers better predict, and possibly postpone, the failure of structures.

"People have been modeling crack growth and fracture for a long time, but the actual process by which it occurs has not really been clear, at least for structural alloys in complicated environments," said Derek Warner, associate professor of civil and environmental engineering and senior author of the work published in Physical Review Letters. "It can be a very large-scale phenomenon—big structures can fracture—but it can be controlled at the atomic scale, particularly when you look at environmental effects."

An environment has many different mechanisms that adversely impact a material, like dissolution, oxide formation, material redeposition, and hydrogen embrittlement. Warner and his team in the Cornell Fracture Group focused on dissolution, which can be found everywhere from corroded metal surfaces to eroded human bone.

The team created a series of atomic 2D models of a structural alloy, similar to aluminum and steel, that was ductile—i.e., pliable enough that it that wouldn't shatter when deformed, as glass does.

By running numerous simulations that stressed the material with a range of loading cycles, the researchers were able to see the different ways the atoms interacted. The researchers then began removing loosely bonded atoms from the surface, one at a time, and monitored the crack's behavior.

They found that removing surface material inhibited the crack from growing.

"The proclivity of a crack to grow depends on how sharp it is," Warner said. "If you have a big round notch, it's unlikely to propagate like a crack. But if you have some sharp feature, like a slit cut with a knife, it is more likely to grow. So in this way, material removal, akin to what occurs during corrosion, can actually improve mechanical performance."

The research is of particular interest for the Office of Naval Research, which funded the study, and its efforts to keep expensive aircraft in safe working condition amid the extreme ocean environment.

For more information: Cornell University www.cornell.edu

Source: ASM International

****

Nalco posts over three-fold jump in December quarter profit at Rs 831 cr

National Aluminium Company Ltd (Nalco) said its December quarter consolidated profit surged over three times to Rs 830.67 crore. The company had posted a profit of Rs 239.71 crore for the year-ago period, Nalco said.

Income during the quarter increased to Rs 3,845.25 crore over Rs 2,414.95 crore in the year-ago period. The company paid final dividend of Rs 1 per equity share amounting to Rs 183.66 crore for 2020-21. With this, the total amount of dividend payout for 2020-21 is Rs 3.50 per equity share -- interim dividend of Rs 2.50 per share and final dividend of Rs 1 per share amounting to Rs 644.27 crore.

Business Standard

Govt revokes anti-dumping duties on certain steel products

The government announced revoking of anti-dumping duties on certain steel products imported from countries including China, a move aimed at containing high prices of metals and promoting domestic manufacturing.

Countervailing duty (CVD) is also being permanently removed on imports of certain hot-rolled and cold-rolled stainless steel flat products from China. "Certain anti-dumping and CVD on stainless steel and coated steel flat products, bars of alloy steel and high-speed steel are being revoked in larger public interest considering prevailing high prices of metals," Finance Minister Nirmala Sitharaman said in her Budget Speech. Engineering exporters have demanded from the government to take steps to control high steel prices.

The Economic Times

Tata Steel Long Products acquires NINL for Rs 12,100 cr

Tata Steel Long Products (TSLPL) aid that it has been identified as the winner of the bidding process to acquire a 93.71% equity stake in Neelachal Ispat Nigam (NINL).

The company's bid has been declared successful in accordance with the process being run by Department of Disinvestment & Public Asset Management (DIPAM), Government of India.

NINL represents a critical and strategic acquisition for TSLPL with around one million tons per annum of steelmaking capacity, 2500 acres of land for future growth and iron ore reserves of around 100 million tons. NINL will become the core of TSLPL's growth aspirations, as it is intended to not only restart the one million ton steel plant expeditiously but also begin work immediately to build a 4.5 million ton per annum state of the art long products complex in the next few years, and further expand it to 10 million ton per annum by around 2030.

As part of the larger Tata Steel ecosystem, the location of the NINL complex presents opportunities to leverage synergies with existing infrastructure, bring to bear best operating practices and expertise in mining as well as project management to create significant value. TSLPL has a clear strategy to build its business across long products, including branded products, downstream solutions and speciality high-end products.

The total consideration of Rs 12,100 crore reflects the enterprise value (including all recorded liabilities) as part of the acquisition of 93.71% equity stake in NINL.

The transaction is scheduled for closure within the next couple of months as per the process timelines announced by DIPAM, Government of India.

Business Standard

Vedanta Aluminium launches 'Restora', India's first low carbon 'green' aluminium

Vedanta Aluminium Business, India's largest producer of aluminium and value-added products, launched 'Restora', its low carbon, 'green'

aluminium brand. The company unveiled two product lines - Restora (low carbon aluminium) and Restora Ultra (ultra-low carbon aluminium) under the brand.

Vedanta Aluminium is the first major non-ferrous Indian metals producer to manufacture low carbon products (primary aluminium) for customers worldwide, exhibiting a strong step towards its commitment of achieving Net Zero Carbon by 2050. Both products have been verified as low-carbon aluminium post assessment by an independent, global verification assurance firm.

With Restora, Vedanta Aluminium will address the fast-growing global demand for low carbon aluminium, driven by greater climate consciousness. Vedanta's Restora is being manufactured at the company's world-class aluminium smelter using renewable energy. Restora has a GHG emission intensity that is well below 4 tonnes of CO2 equivalent (tCO2e) per tonne of aluminium manufactured - the global threshold for aluminium to be considered as low carbon aluminium, and Restora Ultra has an even lower carbon footprint that is amongst the lowest in the world.

Restora Ultra, is made from recovered aluminium through Vedanta's partnership with Runaya Refining, one of India's fast-growing manufacturing startups focussed on creating innovative solutions for the resources sector and leverages patented technology licensed from TAHA International S.A. for processing aluminium dross at Vedanta's plants. Under the Restora Ultra product line, the company will offer aluminium recovered from dross (a by-product of the aluminium smelting process). Restora Ultra is also a testament to Vedanta's sharp focus on 'zero-waste' through enhancement of its operational efficiencies.

The Economic Times

Hindalco PAT jumps 96% in December quarter, stands at Rs 3,675 crore

Hindalco Industries Ltd, Aditya Birla Group's metals flagship, reported a 95.7 per cent jump in consolidated profit after tax (PAT) to Rs 3,675 crore for the quarter ended December 31, 2021.

The results were driven by positive macros and focus on downstream value-added products along with better operating efficiencies.

The company had posted a consolidated PAT of Rs 1,877 crore in the year-ago quarter, Hindalco Industries said in a filing to the BSE. Its consolidated revenue from operations during October-December 2021 increased to Rs 50,272 crore, compared with Rs 34,958 crore in the year-ago period, the filing said.

"Consolidated PAT in Q3 FY22 rose to a record Rs 3,675 crore from Rs 1,877 crore in Q3 FY21, a jump of 96 per cent y-o-y," the company said. Its consolidated revenue for the third quarter stood at Rs 50,272 crore, a jump of 44 per cent as against Rs 34,958 crore, Hindalco added. The company said that it reported its highest net profit in Q3 FY22, surpassing all previous quarterly performances.

The results were driven by a consistent performance by Novelis and an exceptional performance by India business, supported by favourable macros, strategic product mix and an improved performance by the downstream business.

"Novelis continued to report consistent quarterly Ebitda despite challenges in the automotive segment due to the global semiconductor chip shortage, unplanned production downtime in South America and supply chain bottlenecks in Asia," it said.

Ebitda stands for earnings before interest, tax, depreciation and amortisation.

Hindalco Industries Managing Director Satish Pai said, "Our sustained performance and strong balance sheet are driving our plans for further organic capex (capital expenditure). We have already announced over Rs 3,000 crore investments in our downstream pipeline – Hirakud and Silvassa, and the acquisitions of Ryker and Hydro's Kuppam units." Novelis has also announced capital projects that align market growth with sustainability considerations, Pai said.

"An example is the USD 365 million closed-loop recycling and casting centre for the North

American market. Budget 2022 made clear the Indian government's intent and impetus on infrastructure," he said. Pai also said the company expects a surge in demand for aluminium and copper and is well-positioned to serve the market.

Business Standard

Vedanta aluminium production increase by 16% in Q3 FY22

Vedanta Ltd said the cast metal aluminium production at its smelters stood at 5,79,000 tonnes in the third quarter of the current financial, registering an increase of 16 per cent.

"The cast metal aluminium production at our smelters stood at 5,79,000 tonnes in Q3 FY22, higher 16 per cent in comparison to Q3 FY2021 and two per cent as compared to Q2 FY2022," the company said.

The Lanjigarh refinery produced 4,72,000 tonnes of alumina in the third quarter of 2021-22, 16 per cent higher as compared to Q3 FY2021 and eight per cent lower as compared to Q2 FY22. The total production at Zinc-International for the third quarter of FY22 was 52,000 tonnes, 11 per cent lower compared to Q3 FY21.

There was no production in Goa due to the continuation of the suspension of mining pursuant to Supreme Court judgment directing mining operations of all companies in the state to stop with effect from March 16, 2018.

Business Standard

****

MEMBER NEWS

Prof. Dr. RH Tupkary, a Life Member of the Indian Institute of Metals since 1991, is acclaimed expert in iron and steel production in India. He worked as a Lecturer and Reader at BHU and as a Professor and Head of Metallurgical Engineering Department at VNIT, Nagpur. He has written several books in English and Marathi languages on various topics of social sciences. He got an excellent global acceptance because of his two earlier books, one on Modern Steelmaking and the other on Modern Ironmaking.

Recently Dr. Tupkary published four books named :

1. Production of Steel – Theory and Practice
2. Production of Iron – Theory and Practice
3. Science and Technology of Progress
4. Passion in Action – Biographical narration

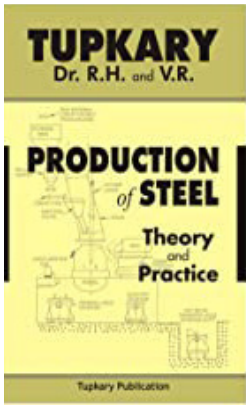

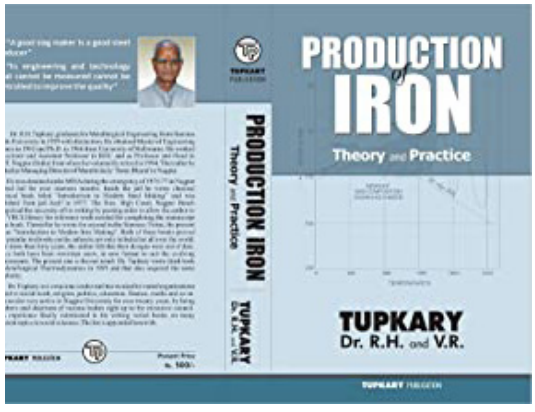

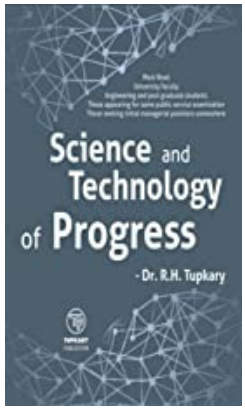

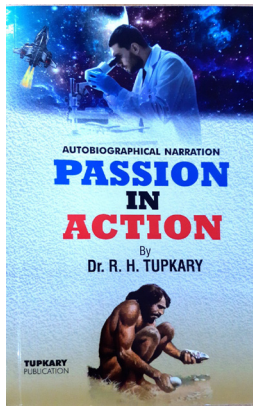

IIM's 75th Foundation Day at Head Office

The 75th Foundation Day was celebrated at the office premises of IIM Head quarter on February 24, 2022. The programme started at 2:30 pm in the auditorium of "Metal House" with a lamp-lighting ceremony by the Chief-guest of the occasion Mr. J. C. Marwah, former Secretary-General, IIM and the welcome song by Ms Nabatara Mitra, IIM HO. Mr. Kushal Saha, the Secretary General, IIM was the convener of the event. The welcome speech was delivered by Mr. Somnath Guha, the Honorary Treasurer of IIM.

After the welcome speech, the delegates shared their reminiscences about "IIM and its journey". Prof. U K Chatterjee shared about his long association with this institute since 1962. He was the Managing Editor of "IIM Metal News" for eight years.

Prof. Shantanu Ray shared about his enduring relationship with IIM from being a reviewer of "IIM Transactions" journal to become the Managing Editor of "IIM Metal News" journal. He also mentioned that he joined IIM as a student member and witnessed the day to day improvement of "IIM Metal News".

Dr. Asim Kumar Ray (Chairman, IIM Kolkata Chapter) shared that he conducted many seminars and technical talks under his leadership. After his retirement, he joined to the Kolkata chapter with a vision to attract the young generation towards the activities of IIM and also wish to induct them in future.

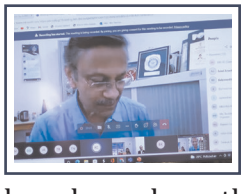

Professor Amol A Gokhale (Immediate former President, IIM) expressed his gratitude to the Indian Institute of Metals and shared that IIM has always been the next most important identity in his career after his primary employment. He always cherished his relationship with IIM since 1986. He also shared his memories and long association with Mr. J. C. Marwah.

Mr. J C Marwah shared that he had a long association of around 23 years with IIM. He worked here for 16 years which included 9 years as the Honorary Secretary and another 7 years as the Secretary-General. He had closely worked with 16 nos. of Presidents of the institute during his tenure. He added, he realised that if he wants to come out with the best result then he has to mould himself with the Presidents as they were the best in their own disciplines of industry/academia/ research. He admitted that each of the Presidents had been a real diamond and that each one had contributed the maximum towards the growth of the institute. He also told "what we see today is because of their leadership", and he hoped that the institute will grow further on the same path they had shown in past.

After the speech of the Chief Guest the cake-cutting ceremony took place to celebrate the 75th Foundation day.

Then, the President of IIM Mr. T. V. Narendran addressed the gathering.

Mr. T. V. Narendran shared that he is delighted to be a part of the 75th IIM's Platinum Jubilee Foundation Day celebration. He stated that IIM has evolved into a very unique institution with a significant impact, and he couldnot think

of any other institution that brings members of the academia, the research and scientific community, together in such a structured manner. IIM organised many commendable events over the years including the recently held National Metallurgists' Day and the Annual Technical Meet which came out as a great platform for the convergence of ideas and thoughts, networking and writing, reaching out across the World.

He also mentioned that the celebration of the Platinum Jubilee year was initiated a year back under the able presidentship of Professor Amol Gokhale, and throughout the year, several events were held. A year-long monthly webinar series were organised across various chapters, special editions of transactions, and an IIM special publication were published to make the 75th anniversary memorable. Two very successful annual technical meets and international conferences were held this year. He thanked Professor Amol Gokhale for conducting it successfully.

After his speech, the monthly webinar series of the Platinum Jubilee Year Celebration was conducted. Prof. Amol A Gokhale, former President of IIM, gave the inaugural speech.

Prof. Gokhale briefed the attendees about the events like monthly webinar series, the logo competition, etc. that were conducted by IIM throughout the year to celebrate its Platinum Jubilee Year. He also shared about the upcoming technical events as a part of this celebration. He thanked the teams who had spent their precious time to organise the events successfully.

After that Dr. Balamuralikrishnan, Scientist, DMRL shared the glimpses of the webinar series through a presentation which was widely accepted by the audience.

The first speaker of the webinar was Dr. Debasish De Sarkar, former Honorary Treasurer, IIM. He shared a presentation on reminiscence of 75 years long journey of IIM. De Sarkar described from the inception of IIM to the every milestone that IIM crossed in the last 75 years, in a lucid manner.

The second speaker of the day was Mr. Bhaskar Roy, former Secretary General, IIM. He delivered the technical talk on the subject "Impact of Climate Change on the Steel Industry". It was well accepted and highly appreciated by all the attendees. An interactive question-answer session made the talk even more attractive.

The event was concluded with a vote of thanks delivered by the Convenor of the event. Ms. Tanisha Neelam Das, IIM HO was the emcee of the event.

Production (unit : Metric Tonne)

	Feb'22	Jan'22	Dec'21	2020 - 21	2019 - 20
ALUMINIUM					
National Aluminium Co Ltd	0.37	0.41	0.40	4.19	4.18
Hindalco Industries Ltd	1.02	1.12	1.11	12.29	13.14
Bharat Aluminium Co. Ltd	0.45	0.49	0.49	5.68	5.63
Vedanta Ltd	1.33	1.46	1.46	14.00	13.43
TOTAL	**3.17**	**3.48**	**3.46**	**36.16**	**36.38**
ZINC (One major producer)					
Hindustan Zinc Ltd	**0.65**	**0.68**	**0.75**	**7.15**	**6.88**
COPPER (Cathode)					
Hindustan Copper Ltd	Nil	Nil	0.0014	Operation Temporarily suspended	0.05
Hindalco (Birla Copper)	0.29	0.33	0.35	2.62	3.26
Vedanta Ltd.	0.11	0.11	0.11	1.01	0.77
TOTAL	**0.40**	**0.44**	**0.4614**	**3.63**	**4.08**
LEAD (One major producer)					
Hindustan Zinc Ltd	**0.14**	**0.16**	**0.16**	**2.14**	**1.81**

Source : https://mines.gov.in/

Prices in India (as on 26th February, 2022)
(Mumbai Local Price in Rs. / kg)

Product	Rs. / kg	Product	Rs. / kg
Copper Armature	731	Brass Shell 40mm	623
Copper cathod LME ++	780	Aluminium 6063 scrap	Not available
CC Rod LME ++	793	Aluminium scrap Taint/Tabor	do
Copper Cable scrap	760	Aluminium Cable scrap	do
Copper shell 40mm	781	Aluminium Ingot	275
Electrolytic Copper strip 25mm	781	Aluminium utensil scrap	197
ACR Copper Coil 3/8	841	Zinc Slab	306
Brass Sheet scrap	550	Lead Ingot	185
Brass Pales scrap	Not available	Tin Slab	3650
Brass Pallu scrap	do	Nickel Cathod	1880
Brass Honey scrap	488		

Source : http://www.mtlexs.com/

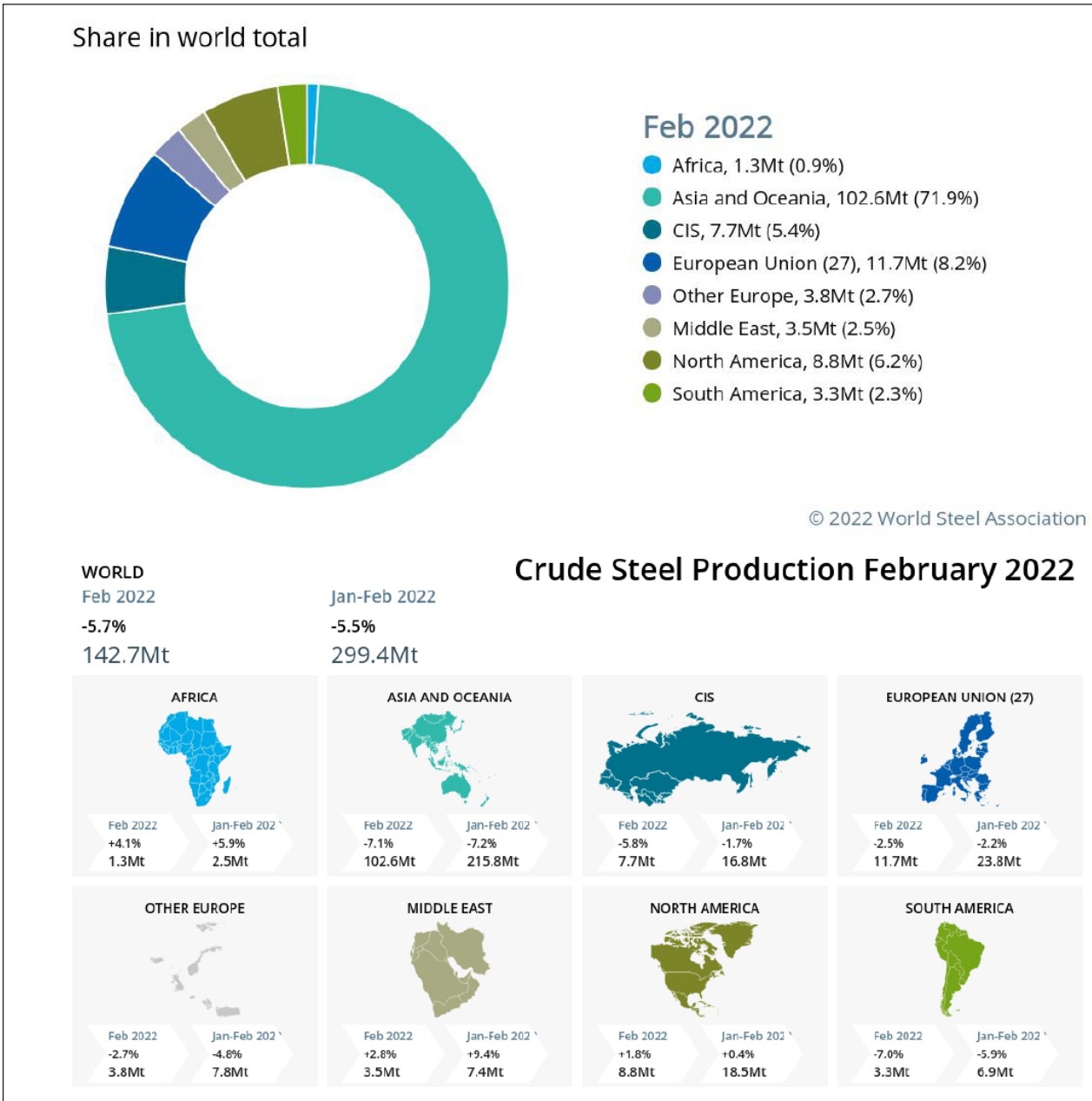

- **Africa:** Egypt, Libya, South Africa
- **Asia and Oceania:** Australia, China, India, Japan, New Zealand, Pakistan, South Korea, Taiwan (China), Vietnam
- **CIS:** Belarus, Kazakhstan, Moldova, Russia, Ukraine, Uzbekistan
- **European Union (27)**
- **Europe, Other:** Bosnia-Herzegovina, Macedonia, Norway, Serbia, Turkey, United Kingdom
- **Middle East:** Iran, Qatar, Saudi Arabia, United Arab Emirates
- **North America:** Canada, Cuba, El Salvador, Guatemala, Mexico, United States
- **South America:** Argentina, Brazil, Chile, Colombia, Ecuador, Paraguay, Peru, Uruguay, Venezuela

Source : World Steel Association